EUROPEAN ORGANIZATION FOR NUCLEAR RESEARCH
CERN - ACCELERATORS AND TECHNOLOGY SECTOR

CERN-ATS-2011-243

Void and Phase Evolution during the Processing of Bi-2212 Superconducting Wires Monitored by combined fast Synchrotron Micro-tomography and X-ray Diffraction

C. Scheuerlein[1], M. DiMichiel[2], M. Scheel[2], J. Jiang[3], F. Kametani[3],
A. Malagoli[3,4], E.E. Hellstrom[3] and D.C. Larbalestier[3]
1 CERN, Geneva, Switzerland
2 European Synchrotron Radiation Facility (ESRF), Grenoble, France
3 Applied Superconductivity Center, National High Magnetic Field Laboratory, Florida State University, Tallahassee, USA

Abstract

Recent study of the current-limiting mechanisms in Bi-2212 round wires has suggested that agglomeration of the residual Bi-2212 powder porosity into bubbles of filament-diameter size occurs on melting the Bi-2212 filaments. These pores introduce a major obstacle to current flow, which greatly reduces the critical current density (J_c). Here we present an in situ non-destructive tomographic and diffraction study of the changes occurring during the heat treatment of wires and starting powder, as well as a room temperature study of ex situ processed wires. The in situ through-process study shows that the agglomeration of residual porosity is more complex than previously seen. Filament changes start with coalescence of the quasi-uniform and finely divided powder porosity into lens-shaped defects at about 850 ^{0}C when the Bi-2201 impurity phase decomposes before the Bi-2212 starts to melt. These lens-shaped voids grow to bubbles of a filament diameter on melting of the Bi-2212 and continue to lengthen and then to agglomerate across multiple filaments while the filaments are in the liquid state. The experiment makes clear why melt processing is vital to developing high J_c and also shows how rearrangement of the residual filament porosity on melting imposes a strong longitudinal inhomogeneity in each filament. Reducing the bubble density is clearly an important path to reaching much higher J_c values in Bi-2212 round wires. Synchrotron micro-tomography is an exceptionally powerful technique for studying the spatial extent of the porosity on a scale of about 2 μm and larger.

Published in Superconductor Science and Technology (2011)

Geneva, Switzerland

December 2011

Supercond. Sci. Technol. **24** (2011) 115004 (10pp) doi:10.1088/0953-2048/24/11/115004

Void and phase evolution during the processing of Bi-2212 superconducting wires monitored by combined fast synchrotron micro-tomography and x-ray diffraction

C Scheuerlein[1], M Di Michiel[2], M Scheel[2], J Jiang[3], F Kametani[3], A Malagoli[3,4], E E Hellstrom[3] and D C Larbalestier[3]

[1] European Organization for Nuclear Research (CERN), CH-1211 Geneva, Switzerland
[2] European Synchrotron Radiation Facility (ESRF), 6 rue Jules Horowitz, F-38043 Grenoble, France
[3] Applied Superconductivity Center, National High Magnetic Field Laboratory, Florida State University, Tallahassee, FL 32310, USA

E-mail: Christian.Scheuerlein@cern.ch

Received 2 August 2011, in final form 3 September 2011
Published 30 September 2011
Online at stacks.iop.org/SUST/24/115004

Abstract
Recent study of the current-limiting mechanisms in Bi-2212 round wires has suggested that agglomeration of the residual Bi-2212 powder porosity into bubbles of filament-diameter size occurs on melting the Bi-2212 filaments. These pores introduce a major obstacle to current flow, which greatly reduces the critical current density (J_c). Here we present an *in situ* non-destructive tomographic and diffraction study of the changes occurring during the heat treatment of wires and starting powder, as well as a room temperature study of *ex situ* processed wires. The *in situ* through-process study shows that the agglomeration of residual porosity is more complex than previously seen. Filament changes start with coalescence of the quasi-uniform and finely divided powder porosity into lens-shaped defects at about 850 °C when the Bi-2201 impurity phase decomposes before the Bi-2212 starts to melt. These lens-shaped voids grow to bubbles of a filament diameter on melting of the Bi-2212 and continue to lengthen and then to agglomerate across multiple filaments while the filaments are in the liquid state. The experiment makes clear why melt processing is vital to developing high J_c and also shows how rearrangement of the residual filament porosity on melting imposes a strong longitudinal inhomogeneity in each filament. Reducing the bubble density is clearly an important path to reaching much higher J_c values in Bi-2212 round wires. Synchrotron micro-tomography is an exceptionally powerful technique for studying the spatial extent of the porosity on a scale of about 2 μm and larger.

(Some figures in this article are in colour only in the electronic version)

1. Introduction

Conductors based on $Bi_2Sr_2CaCu_2O_x$ (Bi-2212) high temperature superconductor are unique in that they can attain high critical current densities in round wire shapes at very high magnetic fields. Fields >30 T are reachable with Bi-2212 magnets [1], which is well beyond the 24 T field limit reachable with Nb_3Sn magnets. The round wire geometry makes the Bi-2212 conductors especially interesting for high energy physics applications where Rutherford cables are preferred for race track windings [2, 3].

[4] Present address: CNR-SPIN Genova, Corso Perrone 24, 16152 Genova, Italy.

At this time the best conventionally processed Bi-2212 wires attain engineering current densities which exceed ~400 A mm^{-2} at 4.2 K and 12 T (~1400 A mm^{-2} in the superconductor) [4], about a factor of two below Nb_3Sn conductors for which the superconductor J_c can attain 2500–3000 A mm^{-2}. Whether the Bi-2212 performance limits are still capable of strong enhancement is thus of great interest. The upper limit to the critical current density (J_c), normally defined by I_c/A_{sc} (I_c is the critical current and A_{sc} is the superconducting cross-sectional area) is always determined by vortex pinning, but the meaning of J_c defined in this way is only very uncertainly connected to the vortex-pinning limit if A_{sc} varies locally. Extensive recent analysis of J_c of Bi-2212 wires concludes that vortex pinning is optimized by a final low-temperature heat treatment (HT) in pure O_2 that overdopes the Bi-2212, raises the irreversibility field (H_{irr}), and reduces the electronic anisotropy [5]. The J_c of typical wires is also enhanced by slow cooling through the resolidification step that follows melting of the Bi-2212 filament bundles [6]. Slow cooling appears to enhance the connectivity of the filament bundle by forming large Bi-2212 grains. Indeed variations of J_c of 3–5 appear to occur without any change in $H_{irr}(T)$, thus pointing to variations of the filament connectivity as the dominant control variable for J_c.

Limitation of J_c by grain boundaries is another expected current-limiting mechanism (CLM), which is also ameliorated by overdoping. Another recent study by Shen *et al* [7] shows that increasing time in the melt state exerts a significantly negative effect on J_c. Indeed Bi-2212 is so complex that many other CLMs may be present. Correlations to process steps are often compromised by the inability of authors to devise experiments without multiple, often hidden variables. The search for the key process variables has thus suffered many detours and frustrations.

In a recent study of the length-dependence of I_c in representative wires, we were surprised to find evidence for long range movement of Bi-2212 in the filament pack which occurs during the vital melt step needed to develop a high I_c [8]. This caused us to focus on the fact that the filaments in any wire made by the powder-in-tube (PIT) process are less than 100% dense because filament deformation depends on powder sliding, shear or fracture. Experiments with monofilaments suggest that the final powder density is only 70–75% [9], while our estimates of today's multifilamentary wires suggest that the as-drawn density prior to reaction is even smaller, of order 60%. If, plausibly, residual air fills the pores, it can expand on melting, producing various negative effects, because only oxygen can pass through the Ag sheath. Kametani *et al* [10] showed that wires quenched from the melt state had frequent filament-diameter bubbles that remained throughout the whole complex I_c optimization process. Gas expansion was also proposed as the reason for the long range movement and density variation observed by Malagoli *et al* [8] in 1 m long wires. Although the bubbles can be bridged by Bi-2212 grains that form on cooling [10], the net result of this major rearrangement of the porosity is to subdivide the length of each filament by voids, which of course locally reduces the wire I_c because the individual filament cross section can be reduced almost to zero, thus forcing current to transfer from one filament to another through Bi-2212 intergrowths or by ohmic dissipation through the Ag matrix. Because of the major and frequent obstruction to the continuity of the Bi-2212 phase within the filaments provided by these bubbles, we have identified them as a major CLM. Indeed a very recent study by Jiang *et al* [11] shows that methods which reduce the pore density allow the I_c of wires to be doubled.

The purpose of the experiments described in this paper was to provide a detailed view of the generation of voids by using non-destructive *in situ* synchrotron micro-tomography and x-ray diffraction to monitor the void (bubble) and phase evolution throughout all stages of the Bi-2212 HT process. Due to the high flux of high energy x-rays available at the ID15A beam line at the European Synchrotron Radiation Facility (ESRF) [12], tomograms of the highly absorbing Bi-2212 samples can be achieved within less than one minute, which enables time-resolved *in situ* tomography during heating cycles of superconducting wires [13] and also prevents metallographic polishing artefacts [14]. Accordingly, the results presented here present a much more detailed picture of the formation and growth of the bubbles than was possible in our earlier metallographic study [10]. Because we believe that voids are a major CLM in multifilamentary Bi-2212 wires, we also believe that the techniques and results presented here will be of great value in developing this unique round wire high temperature superconductor for a new high field magnet technology.

2. Experimental details

2.1. The samples

The wire samples were cut from two PIT Bi-2212 wires (referred to as 'W8' and 'W13'), produced by Oxford Superconducting Technology. Both wires are almost identical except that the monofilaments of the W13 wire were produced in an oxygen environment. The double-stacked 37 × 18 filament wires with an outer diameter of 0.8 mm are composed of 18 sub-elements. Each sub-element contains 37 filaments ~15 μm in diameter. The monofilaments were produced by inserting Bi-2212 precursor powder (see figure 9) into a pure Ag matrix, while the outer sheath is made of Ag–Mg with 0.2 wt% Mg. About 25–28 vol% of the as-drawn, so-called green state wire consists of Bi-2212 and its residual porosity.

A complicating factor for Bi-2212 processing experiments that is only just beginning to be widely appreciated is the question of which sample length produces a representative critical current. Two extremes can be considered: (1) short samples of a few centimetres in which considerable relief of the internal pressure can occur without leaving much variation of the final Bi-2212 density and (2) long coil lengths in which I_c is generally much lower [15]. For the present *in situ* experiments, short samples were imposed by the geometry of the furnace, so the results are representative for the short sample limit only.

All heat treatments that were performed in the synchrotron (in air) are referred to as *in situ* heat treatments. All samples

that were heat treated at the ASC-NHMFL (in pure O_2 atmosphere) are referred to as *ex situ* samples.

2.2. Combined synchrotron x-ray diffraction and micro-tomography during in situ heat treatment

Combined synchrotron absorption micro-tomography and x-ray powder diffraction measurements were performed at the ID15A beam line of ESRF using a monochromatic 69.95 keV x-ray beam with a bandwidth of 0.7 keV. Fast micro-tomography scans were performed using a high resolution imaging detector. The detector consists of a 15 μm thick LuAG:Ce^{2+} scintillator that converts the x-ray absorption signal into a visible light image, which is then magnified by a 10× optics and recorded by a high speed CCD camera (DALSTAR Pantera 1M60). The image pixel size is 1.216 × 1.216 μm^2. The x-ray beam size during tomographic scans is 1.5 × 1.5 mm^2. Thanks to the high flux of high energy radiation provided by the ID15 undulator source, 3D tomographic scans of the changes occurring in Bi-2212 wires could be acquired *in situ* with the monochromatic beam in less than a minute, thus avoiding possible artefacts due to sample movement and to microstructural changes occurring during each exposure. The use of monochromatic radiation instead of white (polychromatic) beam radiation prevents beam hardening effects and improves the contrast between voids, Bi-containing phases and Ag.

The theoretical density of Bi-2212 is 6.62 g cm^{-3} [16]. Due to the porosity mentioned above, the density of the precursor powder in the filaments is significantly lower. The theoretical density of Bi-2201, which can be present as an 'impurity' phase is 7.16 g cm^{-3}. The calculated linear absorption coefficients of Ag, Bi-2212 and Bi-2201 with their theoretical densities at 70 keV are $\mu_{Ag} = 40\ cm^{-1}$, $\mu_{Bi-2212} = 15\ cm^{-1}$ and $\mu_{Bi-2201} = 18\ cm^{-1}$. The absorption coefficients of pure Ag and Ag-0.2% Mg differ by only about 1%.

Diffraction measurements were performed in transmission geometry and Debye–Scherrer diffraction patterns were acquired with a high-efficiency, high-readout-speed area detector (Trixell Pixium 4700). The beam size was reduced to 0.3 × 0.3 mm^2 for diffraction measurements and the sample-to-detector distance was 1219.3 mm.

2.3. The heat treatments

The two wires heat treated at ASC-NHMFL were processed using the HT given in [6] with $T_{max} = 888\,°C$ in pure O_2. One sample was quenched after 12 min at T_{max}, when the sample was in the melt state, while the second sample was fully processed.

In situ heat treatments (HT) were performed in the ID15 resistive tomography–diffraction furnace. There is an estimated uncertainty of the stated temperatures of ±10 °C during the combined tomography/diffraction experiments. Additional XRD measurements were performed with a thermocouple spot welded onto the Bi-2212 wire sample. In this case the sample temperature accuracy was better than ±2 °C.

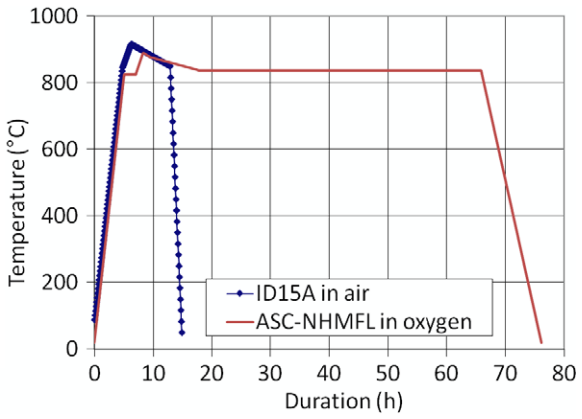

Figure 1. Comparison of the ID15A *in situ* HT (in air) and the ASC-NHMFL HT (in O_2).

Although doing the HT in pure O_2 is currently the preferred route to high J_c, only heating in air was possible for the *in situ* treatments. The ability to combine tomography and XRD in one experiment means, however, that we are able to tie the pore space rearrangements to the key melting and solidification steps occurring during the HT. Thus, doing the HT in air did not compromise the central question of when and why the dramatic changes of the shape and size of individual voids occurred.

Two *in situ* HTs were performed, one to $T_{max} = 875\,°C$ and one to $T_{max} = 915\,°C$, so as to contrast the changes that occur when all of the Bi-2212 powder melts ($T_{max} = 915\,°C$) with those when only a fraction of the powder melts ($T_{max} = 875\,°C$). In order to keep the synchrotron beam time within reasonable limits, the *in situ* HTs were accelerated. The complete temperature cycle to $T_{max} = 915\,°C$ is: ↑160 °C h^{-1} to 845 °C, ↑ 50 °C h^{-1} to 915 °C, → 915 °C–0.2 h, ↓10 °C h^{-1} to 850 °C, ↓400 °C h^{-1} to room temperature (RT). In figure 1 the *in situ* HT cycle in air during which the tomograms were acquired is compared with the ASC-NHMFL schedule in pure O_2. Since the largest changes in the void distribution occur in the melt stage where the differences in the two HT cycles are smallest, we believe that this necessary reduction in time at high temperature occurred without harm to our experimental goals.

One tomogram and one diffractogram were acquired every 5 min. Thus, the temperature resolution of the experiment above 850 °C is about 4 °C (heating) and about 1 °C (cooling).

3. Results

3.1. Phase evolution during Bi-2212 wire processing

An overview of the phase evolution during the processing of the Bi-2212 W8 wire in air can be seen in figure 2, showing the intensity evolution of Bi-2212 and Bi-2201 diffraction peaks that were acquired simultaneously with the tomograms shown later. The evolution of the peak at 1.96 Å characteristic for a phase formed when Bi-2212 melts is shown as well. The diffraction peaks formed when Bi-2212 melts are possibly

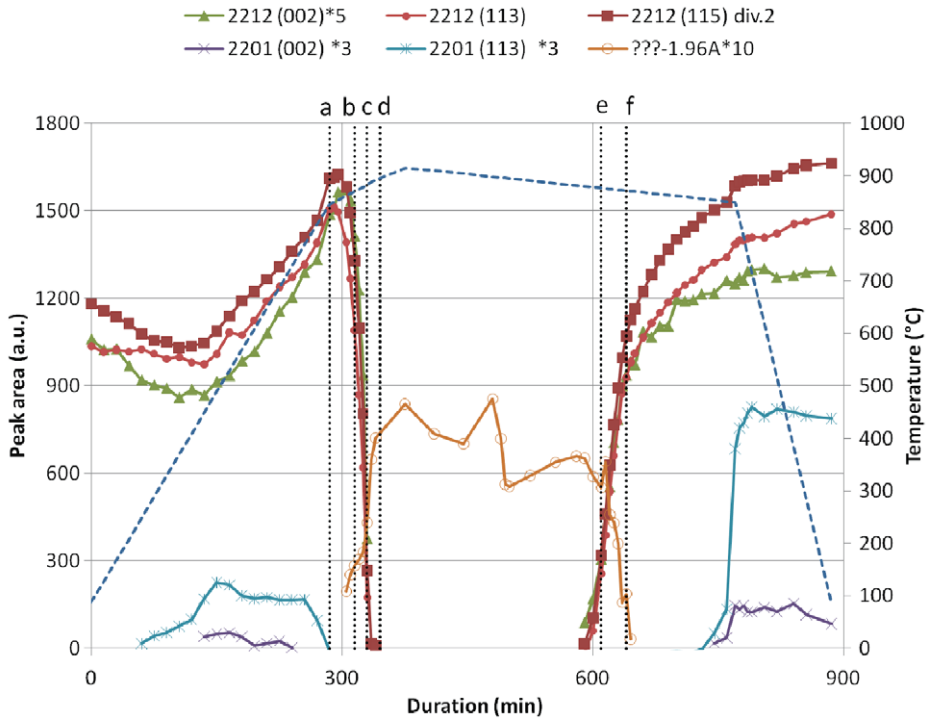

Figure 2. Evolution of Bi-2212, Bi-2201 and 1.96 Å peak areas as a function of duration during *in situ* HT of green W8 wire up to $T_{max} = 915\,°C$. Peak areas have been scaled to fit into the plot. The dotted lines with the annotations 'a'–'f' mark the durations at which the tomograms shown in figure 4 have been acquired.

characteristic for alkaline earth cuprate (AEC) and/or copper-free (CF) phases [17], although they are not yet clearly identified by comparison with reference diffraction patterns. The strongest Bi-2212 (200)(020) peak cannot be used for peak-area measurements because it is superimposed on the Bi-2201 (200)(020) peak.

The initial Bi-2212 diffraction peak growth with increasing temperature is attributed to crystallization of Bi-2212 that was amorphized during the wire drawing process. Bi-2201 is detected during the HT in air when the temperature exceeds approximately 200 °C and a Bi-2201 peak area maximum is reached at about 500 °C. Bi-2201 decomposes completely at 850 °C, and re-forms again upon cooling at approximately 850 °C. The amount of re-forming Bi-2201 may be influenced by the cooling rate and the dwelling step that was omitted during the *in situ* HT (see figure 1). The peak intensities shown in figure 2 are somewhat influenced by thermal lattice motion (Debye–Waller factor), which explains the initial decrease of Bi-2212 diffraction peak areas. Nevertheless, the main phase changes are obvious and can be correlated with the tomographic results described below.

The temperature ranges during which the different phases decompose and re-form could be precisely determined from the sequence of diffractograms that is shown in the surface plot of figure 3. The diffractograms were acquired during the *in situ* HT of a Bi-2212 W13 wire, onto which a thermocouple had been spot welded. The temperature cycle during this HT differed somewhat from those described in figure 1, and it consisted of an additional heating step from 830 to above 900 °C.

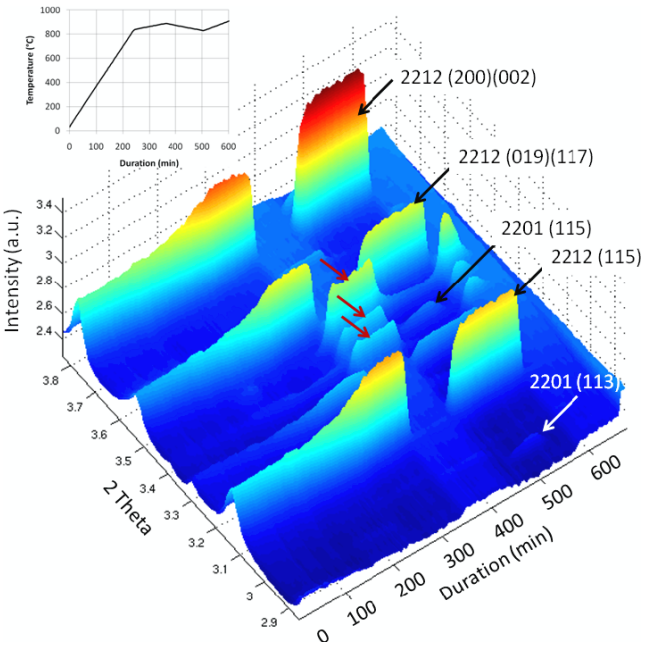

Figure 3. Sequence of diffractograms (log intensity versus diffraction angle 2Θ) acquired during *in situ* HT of W13 wire in air. The diffraction peaks that occur upon Bi-2212 melting are labelled with red arrows. The temperature cycle is shown in the inset.

When heating with a ramp rate of 25 °C h^{-1} in air at ambient pressure the Bi-2212 melts in the temperature range 867–882 °C. Bi-2212 re-nucleation during subsequent cooling

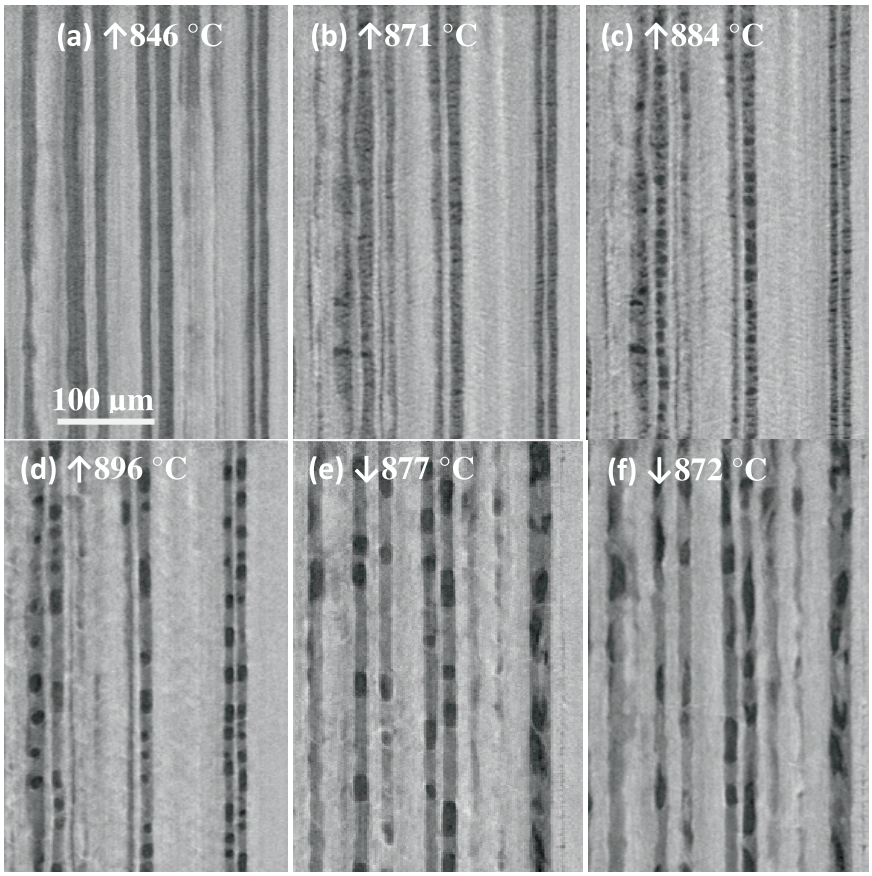

Figure 4. Detailed view of Bi-2212 wire longitudinal tomographic cross sections acquired at different temperatures during an *in situ* HT to $T_{max} = 915\,°C$ in air. A time lapse movie showing the changes occurring over the whole heating and cooling cycle is available (https://edms.cern.ch/document/1153082/1).

is observed in the temperature range 863–842 °C. Bi-2201 is detected during cooling when the temperature decreases below 850 °C.

3.2. Synchrotron absorption micro-tomography

3.2.1. In situ heat treatment to $T_{max} = 915\,°C$ that completely melts the Bi-2212 powder. The evolution of the void distribution during *in situ* HT to $T_{max} = 915\,°C$ can be seen in the longitudinal tomographic cross sections shown in figure 4. In order to show a more detailed view of the voids the images have been cropped from the longitudinal cross sections showing the entire wire cross section. The black areas in the cross sections represent voids, while the bright grey areas the strongly absorbing Ag matrix, and the dark-grey areas are Bi-2212 or other phases that can be formed from Bi, Sr, Ca, Cu and O, like Bi-2201.

No changes were visible in the tomograms on heating from RT to 846 °C. The porosity that is present in the powder is so finely distributed that it cannot be resolved with the tomography experiment, as figure 4(a) shows. However, at 850 °C, where the Bi-2201 diffraction peaks vanish (see phase evolution in figure 2), voids with a size that exceeds the tomographic spatial resolution of about 2 μm first agglomerate. These voids are lens shaped and oriented transverse to the filament direction. With increasing temperature the voids gradually develop a high aspect ratio and expand over the entire filament diameter (see figure 4(b)). The images clearly show a transition from an initially uniformly distributed void space into a quite inhomogeneous distribution that subdivides dense filament regions by very poorly-connected regions.

When the Bi-2212 begins to melt, the size of individual voids increases strongly, and with increasing temperature the void shape changes more and more to a globular shape. At 884 °C (figure 4(c)) where all Bi-2212 is molten (as judged by the vanishing of the Bi-2212 diffraction pattern), all pores have the maximum possible diameter, which is equal to the filament diameter (∼15 μm), and on further heating to 896 °C (figure 4(d)) the voids lengthen. It is striking that about one third of each filament is now occupied by bubbles.

On cooling, the nucleation of Bi-2212 first occurs in the peripheral filaments (figure 4(e) taken at 877 °C), and on further cooling the void contrast so evident in the image taken at 896 °C becomes less marked as voids become partially populated by Bi-2212 grains. However, the residual void space is now very obvious, as is clear by comparing the starting image taken at 846 °C where voids are too small to be visible and the last image taken at 872 °C when many bridged and partially filled voids and also some quite unfilled voids are seen, especially those that elongated while being in the melt state.

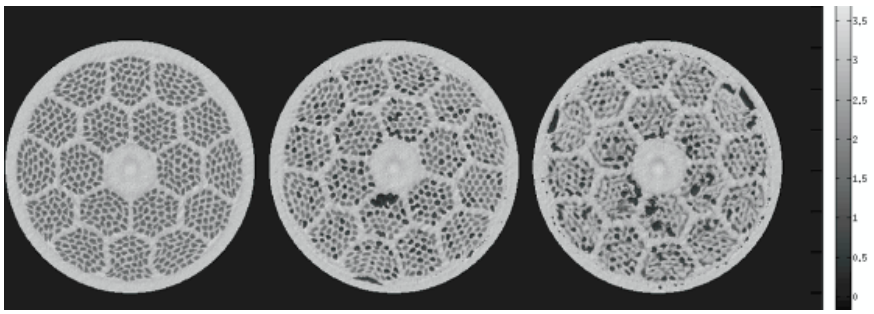

Figure 5. Transverse cross sections of the as-drawn and two samples reacted in 1 bar O_2. From left to right: the as-drawn wire, the wire quenched from $T_{max} = 888\,^{\circ}C$ and the fully processed wire. The change from (an invisible) but homogeneously distributed porosity (before heating) to a very inhomogeneous and now quite visible agglomerated porosity after melting and full processing is very clear. The ROI shown is 620 pixels (754 μm) in diameter, thus slightly cropping part of the Ag–Mg sheath.

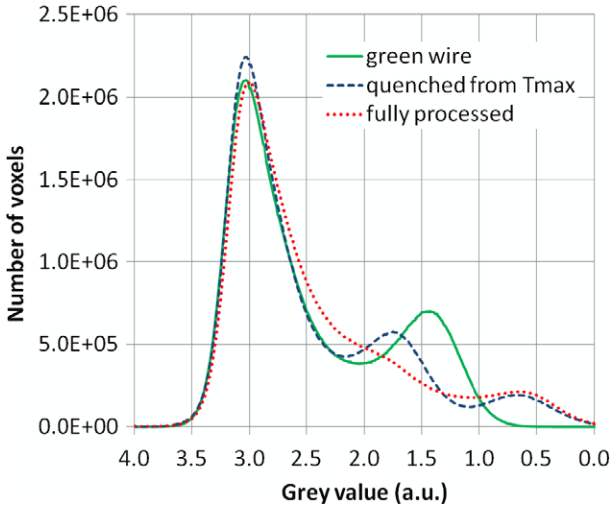

Figure 6. Histograms for the as-drawn (green) and the *ex situ* quenched and fully processed wires. All tomograms were acquired at room temperature.

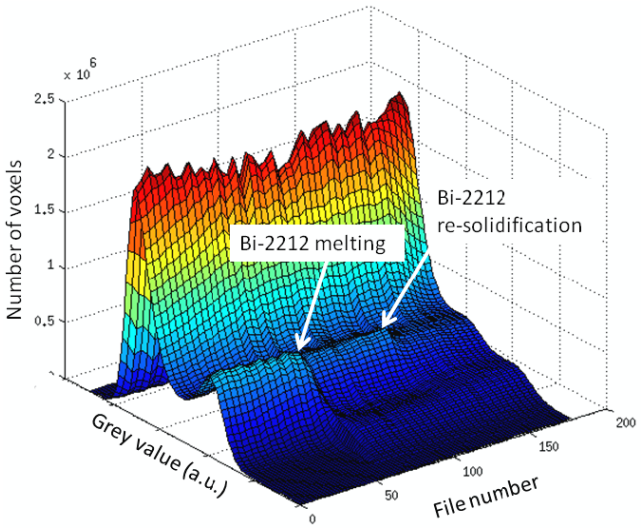

Figure 7. Surface plot showing the 180 grey-scale histograms acquired every 5 min during the *in situ* HT cycle with $T_{max} = 915\,^{\circ}C$ in air.

Figure 5 shows transverse tomographic cross sections of wires in the as-drawn, quenched from T_{max} and fully processed state, the latter two being processed in pure O_2. The images have cropped some of the Ag–Mg sheath so that only the selected region of interest (ROI) of the filament bundles is shown. Consistent with the longitudinal images of the air-processed wires of figure 4, it is again apparent that small voids agglomerate into filament-sized bubbles during the HT and that the net result of the full heat treatment process is to make the void distribution very inhomogeneous.

The corresponding histograms (number of voxels per grey value) are presented in figure 6. In the quenched wire histogram three distinct peaks are seen, which can be attributed to Ag (peak at ~3.0), the Bi-containing phases (peak maximum at ~1.8) and to void space (peak at ~0.6). The grey value maximum of 1.75 corresponds to a linear attenuation coefficient for the Bi-containing phases of roughly 18 cm^{-1}. This is estimated assuming that the grey value maxima of Ag and void space correspond with linear attenuation coefficients of 40 cm^{-1} and 0 cm^{-1}, respectively.

Since the voids in the precursor powder in the as-drawn wire are too small to be resolved, the histogram contains only two peaks. Similarly, in the fully processed wire, the Bi-containing phases are so finely divided that, due to the limited spatial resolution, they do not appear as a distinct peak but as a smeared intensity from about 0.6 to 2.5 in the histograms.

Figure 7 shows all 180 histograms that were acquired during the *in situ* HT ($T_{max} = 915\,^{\circ}C$). The region of interest in which the grey value distribution is determined has a radius of 377 μm (310 pixels) around the centre of gravity, and a length of 792 μm (651 pixels). Three groups can be clearly distinguished, consistent with the three types of histograms shown in figure 6 for as-drawn, quenched from T_{max} and fully processed wires.

The void volume in the non-Ag part of the wire at $T_{max} = 915\,^{\circ}C$ estimated from the grey value distribution in the tomogram is roughly 25%. Due to thermal expansion of the Ag matrix and Ag–Mg sheath, the Ag density and the linear absorption coefficient decreased, which can be seen in figure 7 by a 5.3% shift of the maximum of the Ag peak to a lower grey value when the wire is heated from RT to $T_{max} = 915\,^{\circ}C$.

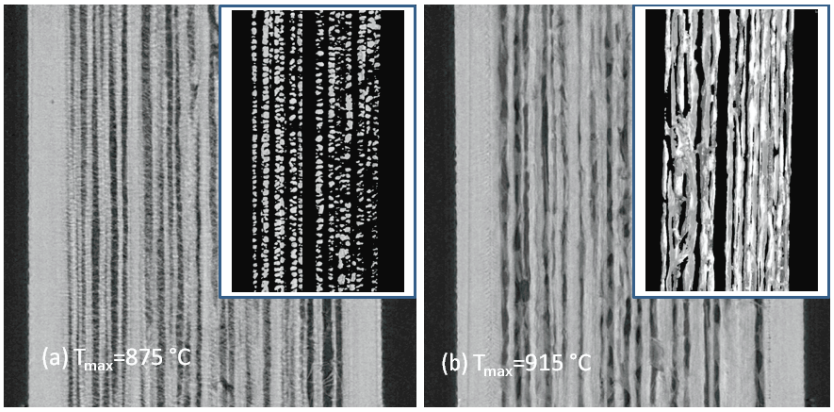

Figure 8. Tomographic cross sections of the Bi-2212 W8 wire acquired at RT after *in situ* HT to (a) $T_{max} = 875\,°C$ and (b) $T_{max} = 915\,°C$. 3D reconstructed images of selected filaments are shown in the insets. In the insets the strand materials have been transparently depicted in order to visualize the pores and the contrast is inversed (pores appear in white).

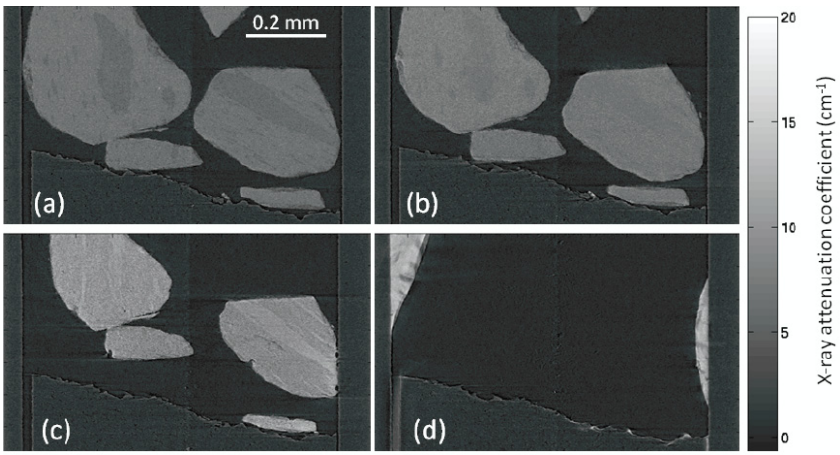

Figure 9. Tomographic cross sections of Bi-2212 powder particles held inside an Al_2O_3 tube during *in situ* HT in air: (a) as-received, (b) and (c) during progressive melting and (d) completely molten.

The Bi-2212 wire diameter at RT and at $T_{max} = 915\,°C$ was measured from the corresponding tomograms. During the *in situ* HT the wire diameter increased by 1.6% from 673 pixels to 684 pixels (corresponding to 0.818 mm and 0.832 mm, respectively). The wire diameters measured at RT before and at the end of the *in situ* HT differ by less than 0.002 mm.

For comparison, the diameters measured for the Bi-2212 W13 wires in the green state and after processing in pure O_2 (quenching from T_{max} to RT and fully processed) are 0.803 ± 0.001 mm, 0.804 ± 0.001 mm and 0.803 ± 0.002 mm, respectively. Diameters were measured with a Beta Laser Mike 283-10 and are average values of at least 24 diameter measurements at three different wire positions. Before HT the wire ends were carefully closed and no leakage was observed.

The fact that, apart from thermal expansion, the wire diameter remained nearly constant indicates that the overall void volume in the short Bi-2212 wire samples remained nearly unchanged during the entire heating cycle.

3.2.2. In situ HT to $T_{max} = 875\,°C$ that only melts a fraction of the Bi-2212 powder. Figure 8 compares tomograms acquired at the end of the full *in situ* HT to $T_{max} = 915\,°C$ with those obtained after a HT at $T_{max} = 875\,°C$, in which only a fraction of the Bi-2212 powder melts. The void space in selected filaments is depicted in the insets of figure 8. The tomograms show very clearly that the completely melted wire has a much more irregular array of long voids, whereas a denser array of rather regularly spaced, lens-shaped voids whose separation is generally of the order of the filament diameter is seen in the tomogram of the wire heated to $T_{max} = 875\,°C$ shown in figure 8(a).

The tomography makes especially clear that even though the critical current is greatly raised by melting of the Bi-2212, the melting step also greatly degrades the filament uniformity. Control of this degradation provides a major opportunity for further optimization of Bi-2212 superconductors, as we take up in the discussion.

3.2.3. Density of the loose precursor powder used in the PIT wire. Tomograms and diffractograms of the Bi-2212 starting powder were acquired during *in situ* HT in air at ambient pressure. These Bi-2212 precursor particles were held inside

a 0.8 mm diameter Al_2O_3 tube. Thanks to the simultaneously acquired diffractograms, the mass density changes described below can be attributed to the partial melting of the Bi-2212 particles. A precise temperature measurement was not possible during this experiment, but Bi-2212 melting occurred at significantly lower temperature than has been observed in the composite wires. The rather low melting temperature of the precursor granulate may be related to the absorption of CO_2 from air [18], and possibly to differences in the oxygen partial pressure [19].

As can be seen from the grey values in the tomographic cross section of the Bi-2212 particles shown in figure 9(a), the attenuation coefficient of 70 keV x-rays varies inside the individual loose powder particles. Attenuation coefficients in the regions with the lowest mass density are about 7 cm^{-1}.

When the powder particles start to melt, as is seen by a strong decrease of the integrated Bi-2212 diffraction peak intensities in the simultaneously recorded diffraction pattern, the volume of the particles shrinks, the x-ray attenuation coefficient increases and the mass density inside the particles becomes more homogeneous (figures 9(b) and (c)). During this densification process the powder particles keep their shape and sharp edges. When Bi-2212 is completely melted (figure 9(d)) the attenuation coefficient approaches 15 cm^{-1}, which is the value calculated for Bi-2212 with the theoretical density of 6.6 g cm^{-3}.

4. Discussion

In recent papers [8, 10, 11], we have laid out several aspects of the large current-limiting effects produced by porosity induced by conventionally optimized melt-processes used for developing high J_c in round wire Bi-2212 conductors. Central to our new definition of the dominant CLMs in such conductors is the finding that residual porosity within the only partially dense filaments agglomerates into bubbles on melting, generating pressure that can move molten Bi–Sr–Ca–Cu–O towards the ends of the wire [8]. This internal pressure causes sheath expansion, can provoke leaks in metre-long samples, and produces a marked depression of I_c and J_c in the middle of such wires [8]. Even in short samples of a few centimetres, filament-sized bubbles subdivide the filaments and do not disappear once formed [10]. However, by reducing porosity by densification replacing the residual gas within the filaments by oxygen, which can pass through the Ag sheath at high temperature, the bubble density was greatly reduced and I_c and J_c doubled [11]. Given the clear importance of controlling bubble formation, the present experiment was designed to follow the redistribution of porosity in normally prepared wires in much more detail than by the previous quenching experiments [10] so as to better understand what happens in this crucial processing step.

This paper describes a simultaneous, non-destructive micro-tomography and x-ray diffraction study which allowed us to follow *in situ* the detailed changes occurring during the processing of state-of-the-art round wire Bi-2212 conductors. By following the phase and porosity changes through the whole melting and resolidification cycle, we were able to discover new features of the porosity rearrangement that occur during normal processing. The experiment confirms that residual porosity in the as-drawn wire agglomerates during melting into filament-sized bubbles, but provides much greater detail about the early stages of porosity agglomeration, which initiates rather earlier than previously thought and is associated with the vanishing of the Bi-2201 impurity phase.

The precursor material used in this work reproduced the best material from composition optimization studies [20, 21]. It was intended to be almost single-phase, but actually contained 2.8±0.5 wt% second phases including 1.2±0.2 wt% Bi-2201 [22]. The study clearly shows that the amount of Bi-2201 in the W8 wire increased during HT in air, that Bi-2201 disappears about 20 °C below the Bi-2212 melt onset, and that on a micrometre scale the void rearrangement first becomes visible in the vicinity of the Bi-2201 vanishing at about 850 °C. This is a new result since earlier *ex situ* experiments led us to conclude that bubbles formed only when the Bi-2212 melts [10].

On continued heating of the wire in air, melting of Bi-2212 in the approximate temperature range 870–880 °C causes further partitioning of the void space, a continuous reduction of void aspect ratio and finally formation of spherical voids. Formation of large spherical voids and their subsequent elongation during prolonged HT was also observed in filamentary Nb_3Sn conductors and was explained to be driven by a reduction of void surface area through coalescence of smaller voids [13].

Image processing of the tomographic Bi-2212 cross sections and diameter measurements of *ex situ* processed Bi-2212 samples show that, unlike Nb_3Sn PIT superconductors, the overall void volume in short Bi-2212 wire samples does not significantly change during the HT. This can be explained both by the fact that Bi-2212 processing does not involve phase transformations associated with important density variations, as is the case for Nb_3Sn conductors [23] and that the samples are short enough to allow some relief of the internal pressure [8].

Above 870 °C, even before major melting of the Bi-2212, most voids extend across the entire filament diameter, thus strongly degrading the Bi-2212 filament connectivity along the wire axis. If the HT is restricted to avoid full melting as with the sample heated only to $T_{max} = 875$ °C, this void distribution remains nearly unchanged during subsequent cooling to RT. Indeed it is commonly observed that a full melting is needed to develop significant J_c in Bi-2212 [21, 24]. The tomogram of figure 8(a) makes it clear that melting is needed to avoid the non-uniform, physical separation of the filament powder structures by the transverse voids that completely interrupt the filament connectivity at many points.

The *in situ* tomograms also show that after the melting of Bi-2212 and its reformation on cooling, the void structure that developed in the liquid state can be partially filled by new plate-like Bi-2212 grains. However, the original void structure remains even in the fully processed wires, leaving unsupported bridges of Bi-2212 that were shown earlier by Kametani *et al*. Comparing the melt state in *in situ* and in *ex situ* processed wires, it can also be seen that voids continue

to grow by agglomeration during the entire time the wire is in the melt state. These observations may provide an alternative explanation for the strong negative correlation between I_c and time in the melt recently observed by Shen *et al* [7]. Although Cu dissolution into the Ag sheath, diffusion to the external surface and removal of Cu as an oxide in the 1 bar O_2 was proposed there, it also seems likely that the increasingly inhomogeneous porosity development generated by increasing time in the melt adds to the degradation of I_c.

The restrictions that were imposed by *in situ* measurements (air rather than pure O_2, relatively short samples, accelerated temperature cycle to different T_{max}) did not compromise comparisons to wires processed in 1 bar of pure O_2 at the ASC-NHMFL. Also, through the combination of tomography and diffraction in one experiment we are able to tie the void changes to the key Bi-2201 and Bi-2212 melting steps and reformation of these phases on cooling.

Comparing the tomograms and histograms acquired *in situ* at T_{max} when Bi-2212 is completely molten, with tomograms taken at RT of wires processed in 1 bar of pure O_2, and quenched from T_{max} shows that the void evolution up to T_{max} is well reproduced during the *in situ* HT, and that the void shape and distribution produced when the Bi-2212 melts is preserved during the quench from T_{max} to RT.

The tomographic histograms acquired after *in situ* processing and full processing in pure O_2 at the ASC-NHMFL show slight differences in the grey value distribution that may indicate that Bi-2212 is more finely distributed in the *ex situ* than in the *in situ* processed wires. The diffractograms acquired for the two wires indicate that some minor peaks are present in each wire that are not detected in the other wire, presumably because the phase equilibria involve different phases, especially different alkaline earth cuprate phases. Nevertheless, the differences in the tomograms and diffractograms of the processed wires are small and the main features of void development in Bi-2212 wires have been well reproduced during the ID15A *in situ* HT.

High energy synchrotron micro-tomography using a monochromatic beam is unique to measure the density variations within single Bi-2212 precursor granulate particles. Further improving the homogeneity of the Bi-2212 granulate prior to its insertion into the composite wires should be beneficial for the performance of the fully processed wires. The origin of the density variations (chemical or mechanical) should be clarified in further studies.

5. Conclusion

The significant changes that occur in the void distribution of as-drawn filaments of unreacted 'green' wires of Bi-2212 as they are heated into the melt state and then cooled to room temperature have been revealed in tomograms acquired during *in situ* HT of recent multifilament Bi-2212 round wires. The initial uniformly distributed porosity changes drastically over a range of temperature from 850 to 890 °C. First agglomeration of void space occurs before the onset of Bi-2212 melting at 850 °C, which is the Bi-2201 decomposition temperature as the simultaneously acquired diffractograms show.

Bi-2212 melting above 870 °C causes further coalescence of void space, a continuous reduction of void aspect ratio and formation of spherical voids. When Bi-2212 re-forms from the melt Bi-2212 grains can partially bridge across these bubbles, but many voids remain even in the fully processed wires. Taken together with the earlier studies of Malagoli *et al* [8] and Kametani *et al* [10] this tomographic study provides firm evidence that agglomeration of large voids during the excursion into the melt state presents a severe current-limiting mechanism in modern round wire Bi-2212 conductors. Elimination of these bubbles has great potential for greatly improving the transport properties of Bi-2212 wires, as indeed has been shown by a recent study by Jiang *et al* that demonstrates that J_c is more than doubled by greatly reducing the residual bubble density [11].

Acknowledgments

We acknowledge the ESRF for beam time on ID15A. We are grateful to Mark Rikel from Nexans SuperConductors GmbH for stimulating discussions and advice. The NHMFL authors thank their colleagues in the Bi-2212 group and in the VHF SMC for lively discussions on the topics of the paper.

The work at the NHMFL was supported by Very High Field Superconducting Magnet Collaboration, an ARRA grant of the US Department of Energy and by the National High Magnetic Field Laboratory which is supported by the National Science Foundation under NSF/DMR-0084173 and by the State of Florida.

References

[1] Weijers H W *et al* 2010 *IEEE Trans. Supercond.* **20** 576–82
[2] Godeke A *et al* 2010 *Supercond. Sci. Technol.* **23** 034022
[3] Godeke A, Cheng D W, Dietderich D R, Hannaford C R, Prestemon S O, Sabbi G, Wang X R, Hikichi Y, Nishioka J and Hasegawa T 2009 *IEEE Trans. Appl. Supercond.* **19** 2228–31
[4] Miao H *et al* 2005 *IEEE Trans. Appl. Supercond.* **15** 2554
[5] Shen T, Jiang J, Yamamoto A, Trociewitz U P, Schwartz J, Hellstrom E E and Larbalestier D C 2009 *Appl. Phys. Lett.* **95** 152516
[6] Shen T, Jiang J, Kametani F, Trociewitz U P, Larbalestier D C, Schwartz J and Hellstrom E E 2010 *Supercond. Sci. Technol.* **23** 025009
[7] Shen T *et al* 2011 *Supercond. Sci. Technol.* at press
[8] Malagoli A, Kametani F, Jiang J, Trociewitz U P, Hellstrom E E and Larbalestier D C 2011 *Supercond. Sci. Technol.* **24** 075016
[9] Karuna M, Parrell J A and Larbalestier D C 1995 *IEEE Trans. Supercond.* **5** 1279
[10] Kametani F *et al* 2011 *Supercond. Sci. Technol.* **24** 075009
[11] Jiang J, Starch W L, Hannion M, Kametani F, Trociewitz U P, Hellstrom E E and Larbalestier D C 2011 *Supercond. Sci. Technol.* **24** 082001
[12] Di Michiel M, Merino J M, Fernandez-Carreiras D, Buslaps T, Honkimäki V, Falus P, Martins T and Svensson O 2005 *Rev. Sci. Instrum.* **76** 043702
[13] Scheuerlein C, Di Michiel M and Haibel A 2007 *Appl. Phys. Lett.* **90** 132510

[14] Scheuerlein C, Di Michiel M and Buta F 2009 *IEEE Trans. Appl. Supercond.* **19** 2653–6
[15] Ghosh A 2011 *BNL* private communication
[16] Schmahl W W, Lehmann M, Raeth S, Gerards M and Riddle R 1998 *Supercond. Sci. Technol.* **11** 1269–76
[17] Zhang W and Hellstrom E E 1995 *Supercond. Sci. Technol.* **8** 430
[18] Zhang W and Hellstrom E E 1994 *Physica* C **234** 137–45
[19] Lang Th, Buhl D and Gauckler L J 1997 *Physica* C **275** 284–92
[20] Miao H, Marken K R, Meinesz M, Czabaj B, Hong S, Rikel M O and Bock J 2006 *Adv. Cryog. Eng.* **52B** 673
[21] Rikel M O *et al* 2006 *J. Phys.: Conf. Ser.* **43** 51–4
[22] Rikel M O 2011 private communication
[23] Di Michiel M and Scheuerlein C 2007 *Supercond. Sci. Technol.* **20** L55–8
[24] Heine K, Tenbrink J and Thoener M 1989 *Appl. Phys. Lett.* **55** 2441–3